



CHORUS

This is the accepted manuscript made available via CHORUS. The article has been published as:

Comparing the same-side ridge in p-p angular correlations at 7 TeV to data measured at the BNL Relativistic Heavy Ion Collider

Thomas A. Trainor and David T. Kettler

Phys. Rev. C **84**, 024910 — Published 22 August 2011

DOI: [10.1103/PhysRevC.84.024910](https://doi.org/10.1103/PhysRevC.84.024910)

Comparing the same-side ridge in p - p angular correlations at 7 TeV to RHIC data

Thomas A. Trainor and David T. Kettler
 CENPA 354290, University of Washington, Seattle, WA 98195
 (Dated: June 27, 2011)

The CMS collaboration has recently reported the appearance of a same-side ridge structure in two-particle angular correlations from 7 TeV p - p collisions. The ridge in p - p collisions at 7 TeV has been compared to a ridge structure in more-central Au-Au collisions at 200 GeV, interpreted by some as evidence for a dense, flowing QCD medium. In this study we make a detailed comparison between 200 GeV p - p correlations and the CMS results. We find that 7 TeV minimum-bias jet correlations are remarkably similar to those at 200 GeV, even to the details of the same-side peak geometry. Appearance of a same-side ridge reflects a change in the sign of the azimuth curvature determined by the ratio of azimuth quadrupole to dipole amplitudes. Extrapolation of quadrupole systematics from 200 GeV suggests that the same-side ridge at 7 TeV is a manifestation of the quadrupole amplitude enhanced relative to the dipole by the energy increase and applied cuts.

PACS numbers: 12.38.Qk, 13.87.Fh, 25.75.Ag, 25.75.Bh, 25.75.Ld, 25.75.Nq

I. INTRODUCTION

The CMS collaboration has recently released the first study of angular correlations from p - p collisions at the Large Hadron Collider (LHC) [1]. A notable result is the appearance of a same-side “ridge” structure possibly related to the expected jet peak at the angular origin (intra-jet correlations). The same-side ridge observed in p - p collisions at 7 TeV has been compared to a ridge structure observed in more-central Au-Au collisions at the Relativistic Heavy Ion Collider (RHIC) [2], interpreted by some as evidence for a dense, flowing QCD medium [3, 4]. The possible correspondence suggests that a dense medium may also form in p - p collisions at 7 TeV.

While the CMS result is intriguing one can ask whether it does indicate novel physics in p - p collisions at LHC energies or is simply an extrapolation of correlation phenomena previously observed at and below 200 GeV. Is the unexpected structure simply explained as the manifestation of an azimuth quadrupole component consistent with RHIC quadrupole systematics extrapolated to 7 TeV and CMS cut conditions?

In the present study we make quantitative comparisons between CMS results at 7 TeV and correlation measurements at RHIC energies. We extrapolate measured RHIC angular correlations to 7 TeV via energy dependence established below 200 GeV and then determine what other alterations of the extrapolated correlation structure are required to describe the 7 TeV data, both minimum-bias data and with cuts applied. Our comparison suggests that phenomenological differences between p - p angular correlations at 200 GeV and 7 TeV are modest. Systematic variations with event multiplicity n_{ch} (within some pseudorapidity η acceptance) and particle transverse momentum p_t at the two energies are quantitatively similar.

We conclude that the difference between a visible same-side ridge at 7 TeV and no apparent ridge at 200 GeV is simply explained. The same-side ridge at 7 TeV results from a competition between the away-side 1D jet peak on azimuth and the nonjet azimuth quadrupole to deter-

mine the net curvature at the azimuth origin. The nonjet quadrupole increases substantially with collision energy above 200 GeV as expected, while the away-side 1D (jet) peak amplitude remains approximately independent of collision energy. The away-side peak is further reduced relative to the quadrupole by the applied n_{ch} and p_t cuts. With greatly-increased collision energy and applied kinematic cuts the same-side curvature changes sign and a same-side ridge emerges.

The paper is arranged as follows. We briefly review the CMS angular correlation results. We then describe general correlation analysis methods applied to nuclear collisions at the RHIC. We review the systematics of angular correlations from 200 GeV p - p collisions. We then report quantitative A-B comparisons between 200 GeV p - p correlations extrapolated to 7 TeV and the CMS results. We conclude that the CMS “ridge” is consistent with RHIC correlation data suitably extrapolated.

II. CMS CORRELATION ANALYSIS

The CMS analysis is directly related to correlation analysis previously carried out at the RHIC. In order to distinguish what is truly novel at the LHC it is important to review quantitative relationships among different analysis methods and the p - p phenomenology that has emerged from previous work at RHIC energies.

A. CMS analysis method

The CMS analysis is based on normalized pair densities

$$S_N = \frac{1}{N(N-1)} \frac{d^2 N^{signal}}{d\Delta\eta d\Delta\phi} \quad (1)$$

$$B_N = \frac{1}{N^2} \frac{d^2 N^{bkd}}{d\Delta\eta d\Delta\phi},$$

where for example N^{signal} is a pair number, to be distinguished from N , the number of (charged) particles in

the angular acceptance. Pair densities S_N and B_N are equivalent to pair numbers \hat{n}_{ab} defined in Ref. [5, 6], with sibling-to-mixed pair ratio $\hat{r}_{ab} = \hat{n}_{ab,sib}/\hat{n}_{ab,mix}$ for 2D bins (a, b) on difference variables $\eta_\Delta = \eta_1 - \eta_2$ (pseudorapidity) and $\phi_\Delta = \phi_1 - \phi_2$ (azimuth). The CMS correlation measure is

$$\begin{aligned} R(\Delta\eta, \Delta\phi) &= \left\langle (\langle N \rangle - 1) \left(\frac{S_N}{B_N} - 1 \right) \right\rangle_N \quad (2) \\ &= (\langle N \rangle - 1) (\langle \hat{r} \rangle - 1), \end{aligned}$$

with the correspondence to measure $\langle N \rangle (\langle \hat{r} \rangle - 1)$ of Refs. [5, 6] established in the second line. The correlation measure defined in Eq. (2) is directly proportional to the specific detector angular acceptance.

Event multiplicity selection strongly influences spectrum and correlation structure in p - p collisions, mainly by biasing the jet frequency per p - p collision [7]. In the CMS analysis p_t -integral angular correlations were obtained for minimum-bias data and for a cut on “offline tracks” $N_{trk} > 110$ ($p_t > 0.4$ GeV/c, $|\eta| < 2.4$) which corresponds to $\langle N_{trk} \rangle = 118$. The corresponding corrected angular density is $dn_{ch}/d\eta \approx 40$. The 7 TeV NSD density is $dn_{ch}/d\eta \approx 5.8$, with $\langle N_{trk} \rangle \approx 16$ [8]. The ratio of cut-selected to minimum-bias corrected multiplicity is then about 7. p_t -differential correlations were also obtained for specific p_t bins. p_t cuts should modify jet correlations and possibly the nonjet azimuth quadrupole. The angular acceptance for the CMS correlation analysis is $(\Delta\eta, \Delta\phi) = (4.8, 2\pi)$ compared to the STAR TPC acceptance $(2, 2\pi)$.

B. CMS correlation measurements

The main CMS results are summarized as follows. Specific correlation histograms are discussed in more detail in Sec. V. The CMS study concluded that jet correlations are enhanced in high-multiplicity collisions. The away-side ridge (interjet correlations) is uniform for $|\eta| < 1.5$, consistent with STAR measurements within the TPC acceptance $|\eta| < 1$ [5, 9]. A CMS breakdown of p - p angular-correlation structure at the LHC can be compared with 200 GeV p - p phenomenology described in Sec. IV.

Several p_t cut intervals were defined. For $p_t \in [1, 3]$ GeV/c and high-multiplicity cut a same-side “ridge” appears. No corresponding ridge is observed in PYTHIA data. The p_t and n_{ch} dependence of the same-side ridge is studied via ZYAM subtraction, usually applied to jet studies with 1D dihadron correlations [10]. The same-side ridge does not depend on charge combinations. A similar structure is observed for correlated γ s from π^0 decay. Observation of a same-side ridge in p - p collisions at 7 TeV and possible implications in relation to a same-side “ridge” reported in more-central RHIC Au-Au collisions are the featured results of the CMS analysis.

III. ANALYSIS METHOD FOR THIS STUDY

We test the hypothesis that the p - p same-side (SS) ridge manifestation at 7 TeV corresponds to a numerical relation between azimuth quadrupole and away-side 1D peak on azimuth (back-to-back jets) amplitudes. For RHIC data we explain why no SS ridge is apparent in p - p collisions, although a significant nonjet quadrupole is measured. We then show why with increased energy and certain applied cuts a same-side ridge can appear in LHC angular correlation data at 7 TeV. The key issue is the interplay of several contributions to the net curvature of angular correlations at the azimuth origin.

We review technical aspects of STAR correlation analysis applied to nuclear collisions at the RHIC. Method details are provided in Refs. [5, 9, 11–16]. We discuss extrapolation of systematics for RHIC energies to 7 TeV. We develop a formalism for describing contributions to same-side curvature from various correlation components. And we discuss methods to compare 2D angular-distribution histograms quantitatively.

A. Correlation measures

For our initial angular correlation analysis we adopted $\langle n_{ch} \rangle (\langle \hat{r} \rangle - 1)$ as the correlation measure, where n_{ch} is the charged-particle multiplicity within the detector angular acceptance $(\Delta\eta, \Delta\phi)$ [5, 6]. Sibling and mixed pair numbers are normalized to unit integral, and pair ratio \hat{r} is averaged over kinematic bins (e.g. multiplicity, p_t , vertex position). That *per-particle* measure is an improvement over conventional *per-pair* correlation function $C \leftrightarrow \langle r \rangle$ or $\langle r \rangle - 1 \rightarrow \Delta\rho/\rho_{ref}$ ($\Delta\rho$ is the correlated-pair density and ρ_{ref} is the reference- or mixed-pair density). The per-particle measure eliminates a trivial $1/n_{ch}$ trend common to all per-pair measures [11]. However, that *extensive* measure is proportional to the specific angular-acceptance product $\Delta\eta\Delta\phi$ defined for the analysis.

The corresponding intensive correlation measure is a form of Pearson’s normalized covariance [11],

$$\frac{\Delta\rho}{\sqrt{\rho_{ref}}} = \frac{\langle n_{ch} \rangle}{\Delta\eta\Delta\phi} (\langle \hat{r} \rangle - 1) \rightarrow \rho_0 (\langle \hat{r} \rangle - 1) \quad (3)$$

assuming single-particle density ρ_0 uniform within the angular acceptance and factorization of the reference density $\rho_{ref} \approx \rho_0^2$. $\Delta\rho/\sqrt{\rho_{ref}}$ is invariant under combination of uncorrelated parts. The correlation measure is independent of angular acceptance if the underlying physical mechanisms are uniform across the acceptance.

B. Transverse-momentum correlations on $\mathbf{y}_t \times \mathbf{y}_t$

2D correlations on p_t or transverse rapidity $y_t = \ln[(p_t + m_t)/m_\pi]$ (m_π for unidentified hadrons) are complementary to 4D angular correlations in 6D two-particle

momentum space. y_t is preferred for visualizing correlation structure on transverse momentum. $y_t \times y_t$ (and angular) correlations can be defined for like-sign (LS) and unlike-sign (US) charge combinations and also for same-side (SS) and away-side (AS) azimuth subregions of angular correlations defined below. Manifestations of different correlation mechanisms (e.g. soft and hard components) can be clearly distinguished in the four combinations of charge-pair type and azimuth subspace [15, 16].

C. Angular correlations on $(\eta_\Delta, \phi_\Delta)$

Angular correlations can be formed by integrating over the entire $y_t \times y_t$ pair acceptance (minimum-bias angular correlations) or over subregions [15, 16]. Examples of the latter include so-called “trigger-associated” dihadron correlations resulting from asymmetric cuts on $y_t \times y_t$.

Two-particle angular correlations are defined on 4D momentum subspace $(\eta_1, \eta_2, \phi_1, \phi_2)$. Within acceptance intervals where correlation structure is invariant on mean position (e.g. $\eta_\Sigma = \eta_1 + \eta_2$) angular correlations can be *projected by averaging* onto difference variables (e.g. $\eta_\Delta = \eta_1 - \eta_2$) without loss of information to form *angular autocorrelations* [6, 11]. The 2D subspace $(\eta_\Delta, \phi_\Delta)$ is then visualized. The notation x_Δ rather than Δx for difference variables is adopted to conform to mathematical notation conventions and to reserve Δx as a measure of the detector acceptance on parameter x . Angular correlations can be formed separately for LS and US charge combinations, as well as for the charge-independent (CI = LS + US) combination [5, 6]. The pair angular acceptance on azimuth can be separated into a same-side (SS) region ($|\phi_\Delta| < \pi/2$) and an away-side (AS) region ($|\phi_\Delta| > \pi/2$). The SS region includes *intrajet* correlations (hadron pairs within single jets), while the AS region includes *interjet* correlations (hadron pairs from back-to-back jet pairs).

D. Two-component p - p angular correlations

Spectra and correlations in nuclear collisions can be decomposed (near mid-rapidity) into soft and hard components, denoting respectively longitudinal fragmentation (mainly diffractive dissociation) of projectile nucleons and transverse fragmentation of large-angle-scattered partons [7, 15–17]. Soft and hard components from p - p collisions are clearly distinguishable in $y_t \times y_t$ correlations, with distinctive forms for each of the LS and US charge combinations and SS and AS azimuth subspaces [15, 16].

The soft component is observed to be localized within $p_t < 0.5$ GeV/c and US pairs (reflecting local charge conservation during projectile-nucleon fragmentation to hadrons). There is some suppression in the SS azimuth region due to local p_t conservation. The SS hard component (jet peak), with $p_t > 0.35$ GeV/c in p - p collisions, is dominated by US pairs (also local charge conserva-

tion during fragmentation), while the AS hard component (jet-jet ridge) has equal LS and US contributions (no interjet net-charge correlation). The soft-component amplitude drops to zero in more-central p - p and Au-Au collisions. The hard-component fraction is a few percent in minimum-bias (NSD) p - p collisions [7] but increases to about one third of the final-state hadron yield in central Au-Au collisions [18].

E. Correlation model functions

The soft component of angular correlations is modeled by a 1D Gaussian on η_Δ with r.m.s. width ≈ 1 . The model is assumed to be uniform on ϕ_Δ for simplicity. The correlation hard component has two parts, a SS 2D peak at the $(\eta_\Delta, \phi_\Delta)$ origin and an AS 1D peak on azimuth uniform on η_Δ (within the STAR TPC acceptance). The SS jet peak (intrajet correlations) is well modeled by a 2D Gaussian. Except for p - p and most-peripheral A-A collisions the AS peak is conveniently modeled as an AS dipole $\propto \cos(\phi_\Delta - \pi)$.

The combined model function including azimuth quadrupole term $\cos(2\phi_\Delta)$ required to describe A-A angular correlations within the STAR TPC angular acceptance $(\Delta\eta, \Delta\phi) = (2, 2\pi)$ is [5, 9, 12]

$$\frac{\Delta\rho}{\sqrt{\rho_{ref}}} = A_0 + A_{2D} e^{-\frac{1}{2}\left\{\left(\frac{\phi_\Delta}{\sigma_{\phi_\Delta}}\right)^2 + \left(\frac{\eta_\Delta}{\sigma_{\eta_\Delta}}\right)^2\right\}} + A_2 e^{-\frac{1}{2}\left(\frac{\eta_\Delta}{\sigma_2}\right)^2} + A_D [1 + \cos(\phi_\Delta - \pi)] / 2 + A_Q 2 \cos(2\phi_\Delta), \quad (4)$$

where a narrow 2D exponential describing quantum correlations and electron pairs from γ conversions [9] has been omitted for clarity. Dipole and quadrupole terms in Eq. (4) are defined differently from those in Ref. [9]. The *nonjet* quadrupole amplitude is expressed in terms of v_2 by $A_Q\{2D\} = \rho_0(b)v_2^2\{2D\}(b)$ [12]. The SS 2D Gaussian term can also be represented as $\rho_0(b)j^2(\eta_\Delta, \phi_\Delta, b)$, defining j^2 as a measure for jet correlations statistically equivalent to v_2^2 for the azimuth quadrupole [18].

For p - p and peripheral A-A collisions the AS dipole term (interjet correlations) may be replaced by a 1D Gaussian on azimuth centered at π with periodic image at $-\pi$ [10]. The total quadrupole component inferred from Eq. (4) then includes the nonjet quadrupole and a possible jet-related quadrupole contribution from the AS 1D peak. For minimum-bias (p_t -integral) angular correlations from A-A collisions the latter amplitude is small, since for r.m.s. widths greater than 1.2 the higher Fourier components of the AS periodic peak array including the quadrupole term approach zero [10].

The minimum-bias SS 2D jet peak in p - p collisions is strongly elongated in the *azimuth* direction, with approximate 2:1 aspect ratio [15, 16]. The strong ϕ elongation in p - p collisions contrasts with strong η elongation in more-central Au-Au collisions, with 3:1 aspect ratio [5, 9].

F. SS ridge and curvatures at the azimuth origin

Appearance of a same-side (SS) ridge depends on the total curvature at the azimuth origin $\phi_\Delta = 0$. A visible ridge is equivalent to a significant negative SS curvature over an extended η_Δ interval. The SS total curvature depends in part on curvature contributions from the AS 1D peak and nonjet quadrupole. Depending on the relative amplitudes of the two components a SS ridge feature may be visible or not. Other contributions to the SS curvature may be present. It is important to distinguish possible appearance of a visible SS ridge from the azimuth quadrupole component which may contribute to its formation *under some circumstances*. We now develop a description of SS curvature systematics.

A closed expression for the SS ($\phi_\Delta = 0$) curvature from a unit-amplitude AS 1D Gaussian periodic peak array with r.m.s. width σ_ϕ (approximated by two Gaussians centered at $\phi_\Delta = \pm\pi$) is given by

$$C(\sigma_\phi) = \left(\frac{\pi^4}{\sigma_\phi^4} - \frac{\pi^2}{\sigma_\phi^2} \right) \frac{2}{\pi^2} \exp\{-\pi^2/2\sigma_\phi^2\}. \quad (5)$$

The SS curvature is negligible for $\sigma_\phi < 0.6$ (Gaussians are fully resolved).

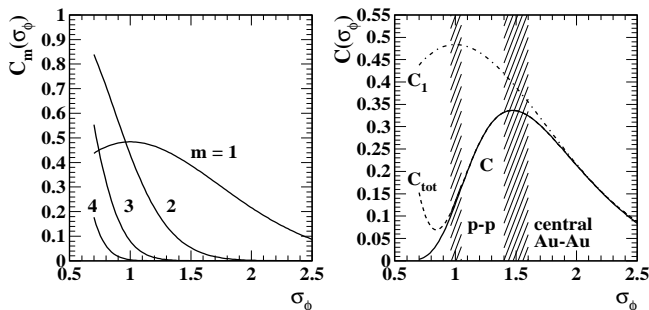


FIG. 1: Left: Same-side curvature contributions C_m from four away-side (AS) 1D Gaussian multipoles $m = 1 \dots 4$ as a function of the AS peak r.m.s. width. Right: Same-side curvature in closed form for an AS 1D Gaussian peak (solid curve) and for Eq. (7) truncated at $m = 3$ (dashed curve). The dipole curvature (dash-dotted curve) is included for reference.

The unit-amplitude AS 1D Gaussian peak array can be expressed as a Fourier series with coefficients given by

$$F_m(\sigma_\phi) = \sigma_\phi \sqrt{2/\pi} \exp\{-m^2\sigma_\phi^2/2\}. \quad (6)$$

The curvature evaluated at $\phi_\Delta = 0$ for an AS 1D peak array with unit amplitude and r.m.s. width σ_ϕ is then given by

$$C_{tot}(\sigma_\phi) = \sum_{m=1} (-1)^{m-1} m^2 F_m(\sigma_\phi), \quad (7)$$

Figure 1 (left panel) shows individual multipole contributions $C_m(\sigma_\phi) = m^2 F_m(\sigma_\phi)$ to the curvature sum in Eq. (7) for $m = 1 \dots 4$. Fig. 1 (right panel) shows the

exact expression C in Eq. (5) (solid curve) and the series in Eq. (7) C_{tot} truncated at $m = 3$ (dashed curve). The deviation from the solid curve is consistent with neglect of the (negative of the) $m = 4$ term in the left panel. The dipole contribution C_1 (dash-dotted curve) is included for reference. The hatched region near $\sigma_\phi = 1$ represents 2D fits to 200 GeV NSD p - p data with an AS 1D Gaussian model. The hatched region near $\sigma_\phi = 1.5$ represents 2D fits to more-central Au-Au data where the AS 1D peak is well modeled by an AS dipole only.

For an AS 1D peak with amplitude A_{1D} and width $\sigma_\phi \geq 1$ (consistent with p - p minimum-bias and Au-Au data) Eq. (7) can be truncated to two multipoles

$$\begin{aligned} C_{AS}(\sigma_\phi) &= B_1(\sigma_\phi) - 4B_2(\sigma_\phi) \\ &\equiv A_D(\sigma_\phi)/2 - 4 \times 2A_Q(\sigma_\phi). \end{aligned} \quad (8)$$

where $B_m(\sigma_\phi) = F_m(\sigma_\phi)A_{1D}$ [10], and 2D fit parameters A_D and A_Q are defined in Eq. (4). An additional (negative) curvature contribution comes from nonjet quadrupole $A_Q\{2D\}$. A SS ridge should appear if the total SS curvature is significantly negative or $16[A_Q(\sigma_\phi) + A_Q\{2D\}]/A_D > 1$. That relation is the central issue for this analysis.

G. A-A vs p - p collision geometry descriptions

A-A collision geometry is described in terms of the Glauber model which relates the A-A differential cross section to participant nucleon number N_{part} and N-N binary-collision number N_{bin} [19]. A derived projectile-nucleon mean path length $\nu = 2N_{bin}/N_{part}$ can also be defined. Through the measured A-A differential cross section on charged-hadron multiplicity n_{ch} within some angular acceptance Glauber geometry parameters are related to the observed n_{ch} .

p - p collision centrality is of significant interest at the LHC [20]. We can in principle relate measured n_{ch} to p - p collision centrality, but we currently have no p - p equivalent to the A-A Glauber model based on participant nucleons. An analogy might be made between participant nucleons in A-A collisions and “participant partons” in p - p collisions derived from the nucleon parton distribution function (PDF). Participant partons, the number depending on p - p centrality or soft momentum transfer, may engage in binary interactions, some of which would result in large-angle parton scattering. Hadron production then arises from projectile-nucleon fragmentation (soft component) and semihard parton scattering to form jets (hard component).

In a two-component study of single-particle p_t spectra from 200 GeV p - p collisions the spectrum hard component was found to scale in amplitude (relative to the soft component) approximately linearly with n_{ch} as n_{ch} was increased by a factor ten relative to the NSD value [7]. The spectrum hard component is quantitatively consistent with minijet correlations [18] and with pQCD-

calculated fragment distributions [21]. The p - p hard-component *absolute* yield increases by a factor 50 as the total particle multiplicity near mid-rapidity increases ten-fold. Equivalently, the jet frequency per p - p collision within one unit of η increases from 2% to nearly 100% [7].

Based on the two-component model we interpret the n_{ch} systematics of spectra and correlations in terms of p - p centrality as follows. For all centralities the soft component arising from longitudinal fragmentation of projectile nucleons comprises no less than 90% of the hadron production, thus defining an “overlap volume” for the p - p collision determined by the large-scale soft momentum transfer. The hard-component *fraction* changes from 2% to 10%, but the hard-component *absolute yield* increases by factor 50, indicating a large increase in the number of participant-parton binary interactions (similar to N_{bin} in A-A collisions). Those systematics suggest that n_{ch} is closely correlated with p - p centrality despite strong event-wise fluctuations in nucleon shape and impact parameter. Increases with n_{ch} are not dominated by jet production but instead by p - p overlap volume.

The overlap of extended (\approx spherical) objects also implies a geometric eccentricity which may be relevant to an azimuth quadrupole in the p - p hadronic final state. We argue by analogy that eccentricity in p - p collisions follows a similar trend to that in A-A collisions, that of two intersecting spheres. The eccentricity of minimum-bias p - p (N-N) collisions may then be approximated by an average over more-peripheral A-A collisions. Just as for A-A collisions the p - p eccentricity may increase initially with increasing n_{ch} (centrality) but then fall off for more-central collisions, the extent depending on the magnitude of geometry fluctuations in p - p compared to Au-Au collisions. We estimate $\epsilon_{opt} \approx 0.3$ for minimum-bias p - p collisions based on ϵ_{opt} centrality dependence for more-peripheral Au-Au collisions [12].

H. 2D histogram A-B comparisons

Angular correlation histograms for this study were binned as 25×28 on $(\eta_\Delta, \phi_\Delta)$ to match the CMS binning. Detailed comparisons of contour lines between data and model functions then permit quantitative inference of model parameters from the CMS data, typically accurate to 10% for the simple structures in p - p correlations. The CMS color palette includes 20 colors, whereas this study employs 50 colors, causing minor differences in shading in some regions but increasing sensitivity. The intervals spanned by vertical scales are nearly the same for model and CMS data in each comparison, although the offsets may differ. By careful A-B comparisons a good approximation to direct χ^2 model fits to histogram data can be achieved. Model uncertainties are discussed in Sec. VI

IV. ANGULAR CORRELATIONS AT THE RHIC

p - p and Au-Au angular correlations at RHIC energies studied extensively by the STAR collaboration [5, 6, 9, 12–16] provide an essential reference for p - p correlation measurements at LHC energies. Minimum-bias jets (minijets) and a nonjet azimuth quadrupole dominate Au-Au angular correlation structure. Minijets play a key role in RHIC collisions [17, 21–23]. Minijet structure is simple in p - p collisions but is strongly modified in more-central Au-Au collisions. The nonjet azimuth quadrupole exhibits simple systematic trends with centrality and energy in Au-Au collisions which are compatible with a nonzero nonjet quadrupole in p - p collisions.

A. 200 GeV p - p model parameters

Figure 2 (left panel) shows the correlation model that describes 200 GeV NSD p - p collisions. The figure was produced from Eq. (4) with parameters summarized below for the STAR intensive correlation measure. Results obtained directly from NSD p - p collisions [15, 16] are consistent with more-peripheral A-A collisions extrapolated to N-N collisions [9], providing a cross check of methods and data consistency. The two cases are thus equivalent.

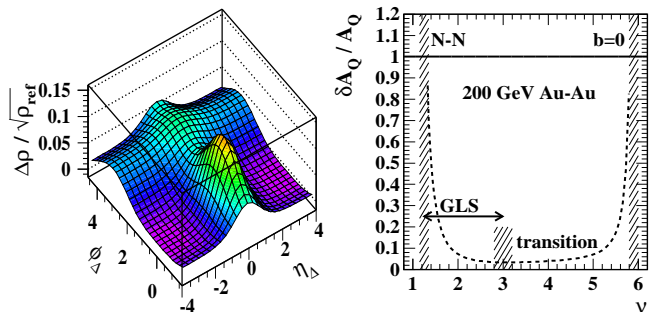


FIG. 2: Left: (Color online) Model angular correlations representing 200 GeV NSD p - p collisions [15, 16]. Right: Estimated error in the nonjet quadrupole component obtained from 2D fits to p - p angular correlations (dashed curve) relative to the quadrupole parametrization in Eq. (9).

The measured 200 GeV p - p /N-N correlation parameters are summarized in the first row of Table I. The SS 2D Gaussian parameters [9] are $A_{2D} = 0.058$, $\sigma_{\eta_\Delta} = 0.64$ and $\sigma_{\phi_\Delta} = 0.9$. The amplitude of the 1D Gaussian on η_Δ is $A_2 = 0.023$, with $\sigma_2 \approx 1$. The AS azimuth dipole amplitude is $A_D \approx 0.046$ (twice the value reported in Ref. [9] because of the different dipole definition). When modeled as a 1D Gaussian the AS peak amplitude goes to $A_{1D} = A_D / F_1(\sigma_\phi) \approx 0.05$, with $\sigma_\phi \approx 1$ implying a significant jet-related quadrupole component. The nonjet quadrupole amplitude extrapolated from Au-Au centrality dependence is $A_Q\{2D\} \sim 0.0005$. The coefficients of the dipole and nonjet quadrupole *sinusoids* are $A_D/2 = 0.023$ and $2A_Q\{2D\} = 0.001$ respectively. The

sinusoid coefficients are important for the curvature discussion in Sec. VII E.

B. Azimuth quadrupole systematics

The azimuth quadrupole, with form $\cos(2\phi_\Delta)$, is conventionally interpreted in A-A collisions to represent “elliptic flow,” a conjectured hydro response in non-central A-A collisions to early development of large pressure gradients [24]. v_2 data inferred from fits to 2D angular correlations and denoted $v_2\{2D\}$ —which accurately exclude contributions from jets (“nonflow”)—reveal systematic behavior inconsistent with hydro expectations, suggesting an alternative interpretation in terms of interacting gluonic fields [25]. Although the azimuth quadrupole is not usually considered relevant to p - p collisions it may explain the CMS SS ridge manifestation.

An analysis of p_t -integral $v_2\{2D\}$ for Au-Au collisions at 62 and 200 GeV, combined with SPS $v_2\{EP\}$ data at 17 GeV, led to the following simple relation which describes $v_2\{2D\}$ data from 13.5 to 200 GeV [12]

$$A_Q\{2D\} = \rho_0(b) v_2^2\{2D\} = 0.0045 R(\sqrt{s_{NN}}) n_{bin} \epsilon_{opt}^2. \quad (9)$$

The product $n_{bin}(b) \epsilon_{opt}^2(b)$ increases rapidly with increasing centrality in Au-Au collisions to a maximum for mid-central collisions (50-fold increase at $\nu \approx 4.5$), beyond which rapidly-decreasing ϵ_{opt}^2 dominates [12].

The nonjet azimuth quadrupole $A_Q\{2D\}$ [introduced as $A_{2\phi_\Delta} \equiv 2A_Q$ in Eq. (4) of Ref. [12]] scales with energy approximately as $\log(\sqrt{s_{NN}}/\sqrt{s_0})$ below 200 GeV, where $\sqrt{s_0} \approx 13.5$ GeV. We therefore define

$$R(\sqrt{s_{NN}}) = \frac{\log(\sqrt{s_{NN}}/13.5 \text{ GeV})}{\log(200/13.5)} \quad (10)$$

as an energy-scaling factor relative to 200 GeV. The energy scaling is based on $\rho_0 v_2^2\{2D\}$ evaluated at $\nu \approx 4.5$ for $\sqrt{s_{NN}} = 62$ and 200 GeV in Fig. 2 of Ref. [12] and SPS $v_2\{EP\}$ data at 17 GeV transformed to the per-particle measure in Eq. (9). The *form* of the $\rho_0(b) v_2^2(b)$ centrality trend for A-A collisions is observed to be independent of collision energy and approximately independent of absolute system size. A significant quadrupole amplitude in p - p collisions is consistent with Eq. (9).

The symbol $R(\Delta\eta, \Delta\phi)$ defined for the CMS analysis (extended to the notation R_X in the present analysis, as in Table I) should be distinguished from energy scaling factor $R(\sqrt{s_{NN}})$ in Eq. (10) which was defined in Ref. [12] in connection with a $v_2\{2D\}$ analysis.

Figure 2 (right panel) provides a basis for estimating the relative uncertainty in the nonjet azimuth quadrupole inferred from p - p collisions at 200 GeV. The nonjet quadrupole estimate is based on a comparison of 2D fits with the AS 1D peak modeled by an AS dipole (zero AS quadrupole component) and a 1D Gaussian (AS quadrupole depending on inferred AS Gaussian width $\sigma_\phi \approx 1$). The dashed curve is the ratio of that difference

to the systematic trend Eq. (9). The nonjet quadrupole uncertainty for N-N (p - p) collisions based on individual 2D fits alone approaches 100%. However, the uncertainty quickly drops to less than 5% within the interval $\nu < 3$ where N-N linear superposition (GLS) is observed to describe Au-Au jet correlations accurately [9].

We argue that a form of linear superposition is also applicable to the azimuth quadrupole, that Eq. (9) may describe the quadrupole amplitude down to N-N collisions, based on arguments presented in Ref. [25]. The quadrupole extrapolation is not based on linear superposition of N-N collisions as in the GLS reference for jet production but rather on the correspondence of overlapping spheres modeling “large-scale” interaction of QCD fields in A-A or N-N collisions. A quadrupole uncertainty estimate based on p - p fits alone is then an overestimate given the accurate Au-Au trend in Eq. (9).

We can apply RHIC Au-Au results to estimate a quadrupole amplitude for p - p collisions at LHC energies. For 200 GeV NSD p - p collisions $n_{bin} = 1$ and we assume $\epsilon_{opt} \approx 0.3$ (Sec. III G), yielding $A_Q\{2D\} = \rho_0 v_2^2\{2D\} \approx 0.0005$. From Eq. (10) we obtain $R(7 \text{ TeV}) = 2.3$. For the CMS analysis additional factors (defined above) lead to $2R_Q \equiv R(7 \text{ TeV}) \Delta\eta \Delta\phi 2\rho_0 v_2^2\{2D\} = 2.3 \times 30 \times 2 \times 0.0005 = 0.07$ as the *predicted* nonjet quadrupole amplitude for minimum-bias p - p angular correlations, consistent with defined CMS correlation measure $R(\Delta\eta, \Delta\phi)$. Systematic uncertainties are discussed in Sec. VI. Increased multiplicity should bias p - p collision geometry to more-central collisions (Sec. III G), suggesting that with increasing p - p multiplicity (centrality) $\rho_0 v_2^2\{2D\}$ may also increase substantially in that system.

C. p - p minijet collision-energy systematics

Jet peak parameters for Au-Au collisions at 62 and 200 GeV are obtained from Ref. [9]. The parameters for the five most-peripheral centrality bins are relevant to this study. The SS and AS peak amplitudes (A_{2D} and A_{1D} respectively) for those bins closely follow a Glauber linear superposition (GLS) trend $\propto \nu$ for $\nu \leq 3$ [9], with $\nu \approx 1.25$ equivalent to minimum-bias N-N collisions [19]. GLS scaling implies that jet correlations for Au-Au collisions within that centrality interval are predicted by jet correlations in p - p collisions, and the reverse. The relative error for each centrality and energy is given by $A_{2D} \pm 7\%$ and $A_{1D} \pm 5\%$.

We base extrapolation of 200 GeV jet correlations to 7 TeV on *quadrupole* energy scaling factor $R(\sqrt{s_{NN}})$ in Eq. (10). The predicted relation between 62 and 200 GeV is $\ln(200/13.5)/\ln(62/13.5) = 1.75$. The observed amplitude ratio for the SS 2D peak averaged over the five most-peripheral Au-Au centrality bins is $1.65 \pm 10\%$, in agreement with Eq. (10). However, the ratio for the AS 1D peak amplitude is $0.95 \pm 7\%$.

The difference between the two cases is consistent with jet systematics. The SS 2D peak amplitude represents

the projected single-jet density on longitudinal rapidity y_z , while the AS 1D peak (AS ridge) amplitude represents the dijet density on 2D space (y_{z1}, y_{z2}) . The two share a common dijet total cross section $\sigma_{dijet}(\sqrt{s})$. Longitudinal rapidity y_z is bounded kinematically by the beam energy $\sim \log(\sqrt{s})$. Since the kinematic bound for the 1D rapidity space goes as $\log(\sqrt{s})$ and that for the 2D space goes as $\log^2(\sqrt{s})$ the difference between SS and AS energy scaling trends may differ by one factor $\log(\sqrt{s})$. In effect, within a fixed detector η acceptance the *fraction* of partner jets falling within the detector acceptance decreases with increasing collision energy, approximately canceling the increase in dijet production. As a consequence the AS 1D peak amplitude is approximately energy independent. The substantial difference in energy scaling between AS 1D peak and azimuth quadrupole amplitudes is of central importance to appearance of the SS ridge at LHC energies but not at RHIC energies (see Sec. VIII E).

D. p - p minijet multiplicity and p_t systematics

Jet angular correlations in p - p collisions scale with n_{ch} as follows (consistent with spectrum hard-component trends from Ref. [7]). The mean jet fragment multiplicity (~ 2.5 , dominated by 3 GeV jets) does not change significantly with p - p n_{ch} (the number of correlated pairs per jet is fixed), but the jet frequency increases by a factor 50 with $10\times$ increase in n_{ch} , rising to about one dijet per p - p collision. Jet correlations measured by $\rho_0 j^2$ then scale up as $10 \times (50/10^2) = 5$, since pair ratio j^2 represents correlated pairs / reference pairs.

For p - p correlations on $y_t \times y_t$ at 200 GeV [15, 16] the SS jet correlation structure (single 2D peak) extends down to $p_t \approx 0.35$ GeV/c, with mode at 1 GeV/c. Nearly half the SS-correlated pairs appear below the mode. In contrast, AS correlations are cut off near 0.7 GeV/c due to initial-state k_t effects. Thus, a smaller fraction of AS pairs appears below 1 GeV/c. For $p_t \in [1, 3]$ GeV/c cuts at 7 TeV imposed on corresponding angular correlations the SS 2D peak amplitude should be reduced approximately by factor 1/3 and the AS 1D peak reduced by factor 1/2.

V. p - p ANGULAR CORRELATIONS AT 7 TEV

We compare minimum-bias angular correlations at RHIC energies to equivalent results from 7 TeV p - p data. Comparison of jet correlations from minimum-bias p - p collisions for the two cases tests an assumed energy extrapolation of RHIC data. We also compare responses to applied n_{ch} and p_t cuts. Correlation parameters for two energies and several cut conditions are summarized in Table I. Comparison of quadrupole and jet extrapolations to CMS data tests the hypothesis that the SS ridge in 7 TeV p - p data results from a combination of nonjet quadrupole and AS dipole structure in angular correlations.

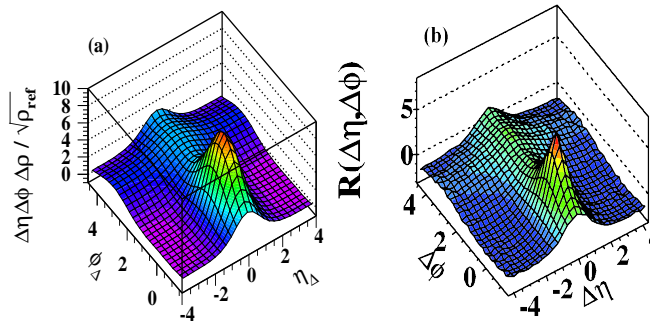


FIG. 3: (Color online) (a) The parametrization of 200 GeV p - p data from Fig. 2 (left panel) rescaled by energy-dependent factor $R(7 \text{ TeV}) = 2.3$ and CMS acceptance factor $\Delta\eta\Delta\phi$. The AS ridge is not scaled up by the energy factor. (b) CMS angular correlations for minimum-bias 7 TeV p - p collisions [1].

A. Minimum-bias angular correlations

Energy extrapolation of minimum-bias nonjet azimuth quadrupole amplitude $A_Q\{2D\}$ to 7 TeV follows Eq. (10) established below 200 GeV, and extrapolation of the corresponding SS 2D peak amplitude A_{2D} follows the same trend. We then scale those 200 GeV parameters A_X (X represents model elements $2D$, Q , D) to CMS results at 7 TeV as $R_X = [R(7 \text{ TeV}) 2\pi\Delta\eta] A_X$, with $R(7 \text{ TeV}) = 2.3$ and $\Delta\eta = 4.8$, or $R_X \approx 70A_X$. As noted in Sec. IV C, energy variation of the AS 1D peak amplitude near 200 GeV is consistent with no change with energy. Only the acceptance factor is include and $R_D \approx 30A_D$. The resulting extrapolation in Fig. 3 (left panel) compares well with CMS minimum-bias data in the right panel. The large ϕ elongation (2:1) of the SS 2D peak observed in 200 GeV p - p collisions [16] seems to persist in 7 TeV collisions, as does the 1D Gaussian on η_Δ associated with longitudinal projectile-nucleon fragmentation [15].

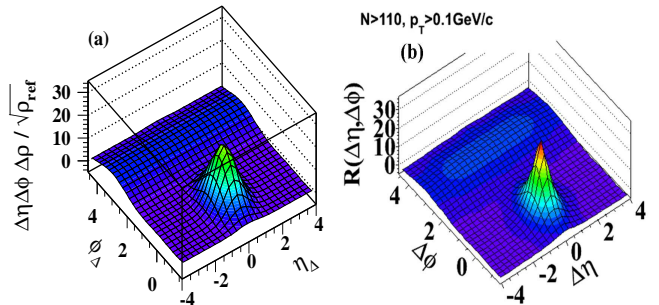


FIG. 4: (Color online) (a) Model function from Fig. 3 (left panel) with jet structure increased by factor 3 and quadrupole increased by factor 6, with SS peak narrowed on η_Δ and with 1D η_Δ Gaussian removed. (b) CMS p_t -integral angular correlations for high-multiplicity 7 TeV p - p collisions [1].

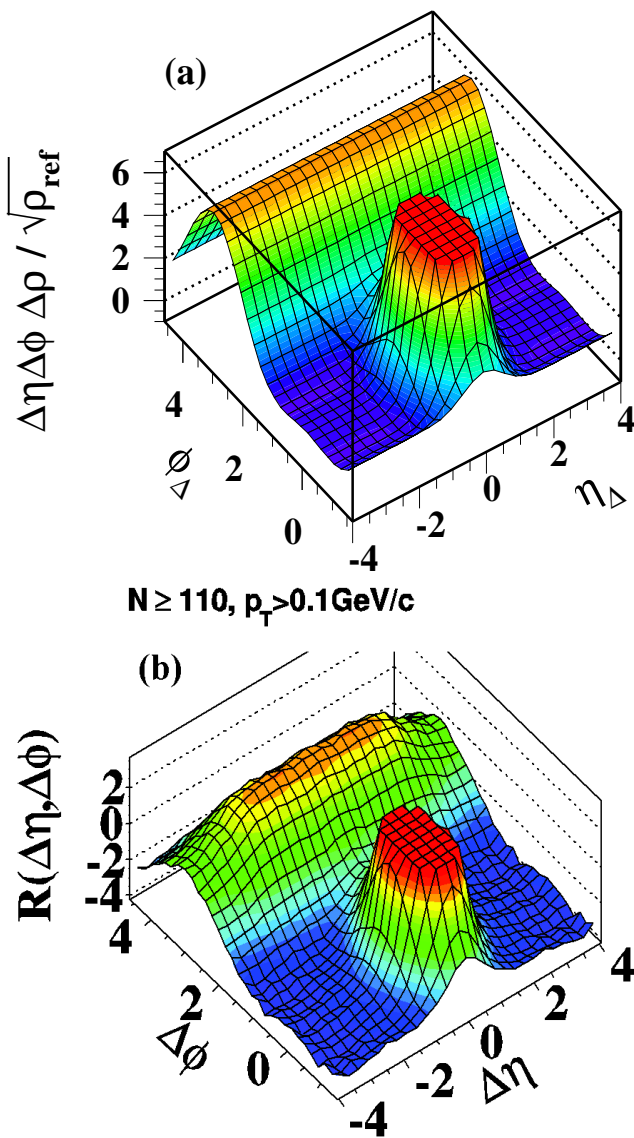


FIG. 5: (Color online) Histograms from Fig. 4 rescaled by factor 5. (a) Model function from Fig. 4 (left panel) with the same quadrupole amplitude $R_Q = 0.42$. (b) CMS p_t -integral correlations for high-multiplicity cut [1].

B. High-multiplicity cut

Figure 4 (left panel) shows the model function in Fig. 3 (left panel) with the following changes: (i) The SS 2D peak amplitude is scaled up by factor 3, (ii) The AS 1D peak amplitude is scaled up by factor 4, (iii) the SS peak ϕ width is reduced from 0.9 to 0.65 and the η width from 0.64 to 0.58, and (iv) the 1D η Gaussian is eliminated. Those changes relative to the minimum-bias case are required to achieve agreement between model and data in this figure and in Fig. 5. The extrapolated jet structure in the left panel compares well with CMS data in the right panel with the exception of the narrow contribution from quantum correlations and electron pairs at the

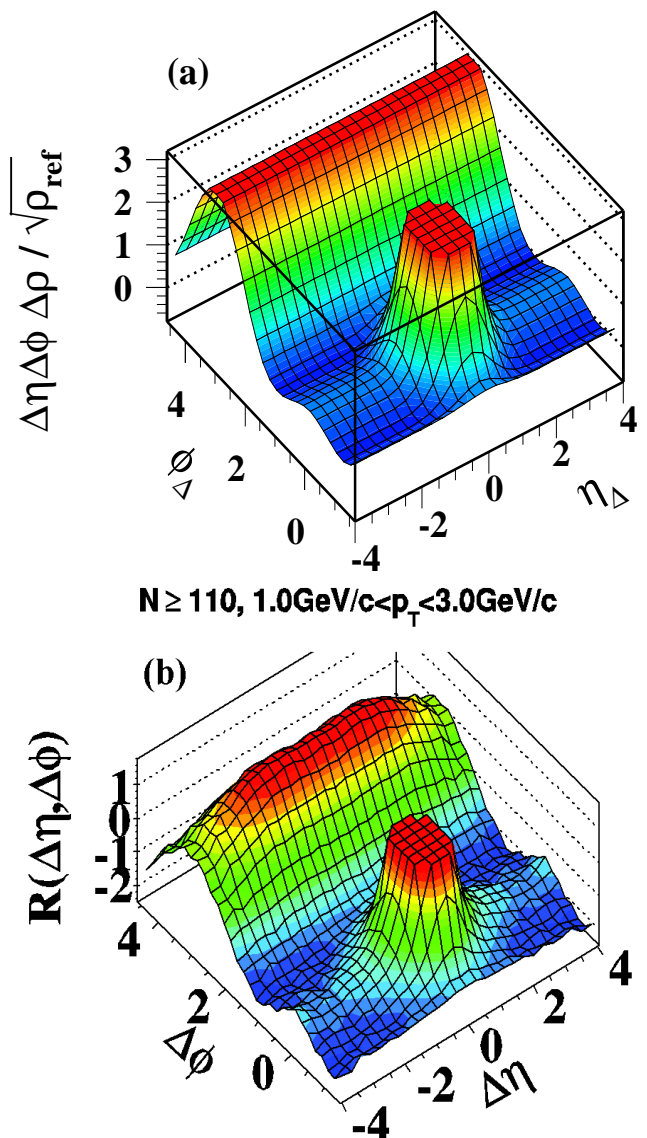


FIG. 6: (Color online) (a) Model function from Fig. 5 (upper panel) with the same quadrupole amplitude but with jet correlation amplitudes and peak widths reduced (see text). (b) CMS correlations for high-multiplicity cut and $p_t \in [1, 3] \text{ GeV}/c$ [1].

peak not included in the model.

Selecting high-multiplicity p - p collisions biases the jet frequency per event to larger values [7]. As argued in Sec. III G the increased hard scattering can be interpreted as the result of increased p - p centrality induced by the multiplicity cut. For 200 GeV p - p correlations a similar multiplicity cut increases jet correlation structure by a factor 5 [15] compared to factor 3 noted for the SS 2D peak in 7 TeV data. The difference is discussed in Sec. VII B.

Figure 5 shows the results in Fig. 4 with the vertical axis range reduced by a factor 5 to enhance small-amplitude details. Correspondence of the SS jet peaks

near the base is evident. The AS ridge shows significant reduction in the data at larger η_Δ (lower panel) which is not included in the model function (upper panel) inferred within the STAR TPC acceptance. The approximately 20% falloff at larger η_Δ is not critical to this analysis.

The nonjet-quadrupole amplitude is increased by factor 6 for this figure to $2R_Q\{2D\} = 0.42$ (relative to the extrapolated minimum-bias value). The larger quadrupole amplitude is required to change the SS curvature in $|\eta_\Delta| > 2$ from concave upward (positive curvature) to slightly concave downward (negative curvature). The 6-fold quadrupole increase is thus already required by CMS data prior to imposition of p_t cuts. The SS curvature issue is further discussed in Sec. VII E.

C. High-multiplicity plus high- p_t cuts

Figure 6 (upper panel) shows the model in Fig. 5 (upper panel) with the following changes: (i) The ϕ width of the SS 2D peak is further reduced from 0.65 to 0.55 leading to a symmetric SS peak, (ii) The SS peak amplitude is reduced by factor 1/3 and AS 1D peak by factor 1/2 compared to the high-multiplicity cut alone and (iii) the nonjet quadrupole amplitude remains approximately the same as for the high-multiplicity cut alone— $2R_Q\{2D\} = 0.42$ increased by factor 6 from minimum-bias 0.07. Although $v_2(p_t)$ is observed to increase rapidly with increasing p_t the p_t -differential quadrupole amplitude $A_Q(p_t, b) = \rho_0(p_t, b) v_2^2(p_t, b)$ used in this study includes as a factor the hadron p_t spectrum which falls rapidly with p_t . Thus, slow variation of A_Q with p_t over some p_t interval is not unexpected.

Those changes provide good agreement between model (upper panel) and CMS data (lower panel), especially near the base of the SS 2D peak. With high- p_t cuts we expect to eliminate some fraction of the jet contribution and possibly to change the quadrupole amplitude. The required changes in jet structure at 7 TeV agree well with the effects of reduced p_t acceptance for jet-correlated pairs at 200 GeV [15, 16]. Appearance of the SS ridge in relation to factors affecting the SS curvature is further discussed in Sec. VII E.

VI. SYSTEMATIC UNCERTAINTIES

We estimate systematic uncertainties for (i) jet extrapolations from RHIC correlations compared to CMS data, (ii) azimuth quadrupole extrapolations and (iii) the A_Q/A_D ratio and manifestation of a SS ridge. The hypothesis to be tested is whether a nonzero *nonjet* quadrupole component in p - p correlations plus a specific cut system is consistent with the SS ridge at 7 TeV.

A. Extrapolating 200 GeV p - p minijet correlations

Jet peak parameters for Au-Au collisions at 62 and 200 GeV are obtained from Ref. [9]. The parameters for the five most-peripheral centrality bins are relevant to this study. The relative uncertainties for those centralities at 200 GeV are represented by $A_{2D} \pm 7\%$ and $A_D \pm 5\%$ based on recent refinement of uncertainties ($\pm 9\%$) given in Ref. [9]. The predicted relation between 62 and 200 GeV by Eq. (10) is $\ln(200/13.5)/\ln(62/13.5) = 1.75$. The observed amplitude ratio for the SS 2D peak averaged over the five most-peripheral bins is $1.65 \pm 10\%$. However, the amplitude ratio for the AS 1D peak is found to be $0.95 \pm 7\%$.

Uncertainties from 62 and 200 GeV measurements are combined with those for the energy extrapolation factors to obtain the final uncertainties. The expected ratio relating 200 GeV and 7 TeV is $\ln(7000/13.5)/\ln(200/13.5) = 2.3$. Scaling the uncertainties established for ratios inferred from RHIC data we expect the SS peak amplitude to increase by factor $2.3 \pm 15\%$ and the AS ridge amplitude to remain unchanged, with factor $1 \pm 10\%$ for 7 TeV relative to 200 GeV. Combining the above results the relative errors for the extrapolated amplitudes at 7 TeV are then represented by $A_{2D} \pm 18\%$ and $A_D \pm 12\%$. We observe in Figs. 4 and 5 that the SS 2D peak amplitude extrapolation is consistent with CMS data, but the AS 1D amplitude requires an additional factor 4/3 to describe the data in Figs. 5 and 6, exceeding the factor-1 extrapolation from RHIC energies (with uncertainty) by 20%.

B. Extrapolating Au-Au quadrupole correlations

The total η_Δ -independent quadrupole in p - p 2D angular correlations within the STAR TPC includes a nonjet quadrupole and the second Fourier component of the AS 1D jet peak, $A_Q = A_Q\{2D\} + A_Q(\sigma_\phi)$ [10]. The total quadrupole can be accurately determined in 2D fits to p - p correlations if the AS 1D peak is modeled as a dipole ($\sigma_\phi \sim \pi/2$). The fitted quadrupole then serves as an upper limit to the nonjet quadrupole. But the nonjet quadrupole in that case has a large uncertainty because of uncertainty in the AS 1D peak width. Since the $A_Q\{2D\}$ trend in Eq. (9) becomes small for peripheral (and central) collisions the relative systematic uncertainty in the nonjet quadrupole inferred from p - p data alone becomes large there, as shown in Fig. 2 (right panel).

The nonjet quadrupole in p - p collisions is better determined by extrapolation from peripheral Au-Au collisions. The nonjet quadrupole in Au-Au collisions at and below 200 GeV has the simple and accurate parametrization shown in Eq. (9) over the complete Au-Au centrality range [12]. Uncertainty in the nonjet quadrupole for p - p collisions can be substantially reduced by extrapolation of the well-defined Au-Au trend to N-N collisions *assuming that such an extrapolation is valid* (Sec. III G). The

TABLE I: p - p correlation systematics. Entries represent systematics inferred from RHIC data at 200 GeV and parameters inferred by modeling CMS angular correlation histograms at 7 TeV from Ref. [1]. The left columns indicate collision energy and cut conditions, including minimum-bias (MB) data. The A_X represent parameters from STAR per-particle analysis with an intensive correlation measure. The R_X represent corresponding CMS data including extensive acceptance factor $2\pi\Delta\eta \approx 30$. Systematic uncertainties for R_X can be obtained from those for A_X by applying the same factor. The pairs of entries in the $2A_{Q,tot}$ and $2R_{Q,tot}$ columns correspond to nonjet and jet-related (AS peak) quadrupoles respectively as described in Sec. VID.

\sqrt{s} (TeV)	Condition	$100 \times 2A_{Q,tot}$	$A_D/2$	A_{2D}	$16A_Q/A_D$	$2R_{Q,tot}$	$R_D/2$	R_{2D}	σ_η	σ_ϕ
0.2	MB	$0.10 \pm 0.025 + 0.23 \pm 0.023$	0.023 ± 0.002	0.058 ± 0.01	0.57 ± 0.16	$0.03 + 0.069$	0.69	1.74	0.64	0.9
7	MB	$0.23 \pm 0.06 + 0.23 \pm 0.023$	0.023 ± 0.002	0.13 ± 0.025	0.80 ± 0.22	$0.07 + 0.07$	0.69	4.0	0.64	0.9
7	n_{ch} cut	$1.40 \pm 0.35 + 0.92 \pm 0.09$	0.092 ± 0.009	0.39 ± 0.08	1.01 ± 0.28	$0.42 + 0.29$	2.9	12.0	0.58	0.65
7	p_t, n_{ch} cuts	$1.40 \pm 0.35 + 0.47 \pm 0.05$	0.047 ± 0.005	0.13 ± 0.025	1.59 ± 0.44	$0.42 + 0.14$	1.45	4.0	0.55	0.55

assumption is tested by comparing the quadrupole extrapolation from RHIC data to LHC p - p data.

Au-Au quadrupole data at 62 and 200 GeV typically agree with Eq. (9) within 10%, consistent with estimated systematic uncertainties. We increase the uncertainty in the extrapolation to N-N collisions to 20%, compared to the nearly 100% uncertainty from 2D fits to p - p data alone. The energy extrapolation by factor 2.3 is assigned the same 15% uncertainty as for mini-jets. The 200 GeV absolute uncertainty is then indicated by $2A_Q\{2D\} = \rho_0 v_2^2\{2D\} \approx 0.001 \pm 0.00025$. Extrapolation to the CMS R measure at 7 TeV is $2R_Q \equiv R(7 \text{ TeV}) \Delta\eta\Delta\phi 2A_Q\{2D\} = 2.3 \times 30 \times 0.001 = 0.07 \pm 0.018$.

C. Model parameters from CMS histograms

Reasonably accurate 2D model parameters can be inferred by visual A-B comparison of 2D histograms if the binning scheme, color palette and vertical axis scales are carefully matched. Critical model parameters are AS dipole amplitude A_D , SS 2D peak amplitude A_{2D} (and peak widths) and quadrupole amplitude A_Q .

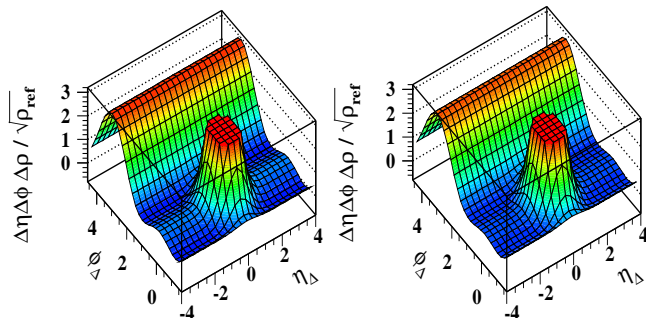


FIG. 7: (Color online) (a) The parametrization of 200 GeV p - p data from Fig. 2 (left panel) rescaled by energy-dependent factor $R(7 \text{ TeV}) = 2.3$ and CMS acceptance factor $\Delta\eta\Delta\phi$. The AS ridge is not scaled up by the energy factor. (b) CMS angular correlations for minimum-bias 7 TeV p - p collisions [1].

Figure 7 illustrates estimation of parameter uncertainties by varying the parameter in question about the optimum until the fit is visually degraded, which typically

overestimates uncertainties derived from χ^2 fits by a factor 2. Figure 7 (left panel) is the upper panel of Fig. 6. The 200 GeV p - p nonjet quadrupole amplitude extrapolated to 7 TeV has been increased by a factor 6 to accommodate the n_{ch} trend of CMS data.

Figure 7 (right panel) is the same model with the factor 6 reduced to factor 4. The result is a quite visible reduction in the SS ridge and a (less obvious) reduction of the apparent AS 1D peak height. The altered model clearly does not describe the CMS data. We thereby estimate the uncertainty in the increase factor by 6 ± 1 . The AS 1D peak amplitude increase factor is 3 ± 0.3 . 10% changes in jet-structure amplitudes are easily detected based on color and shape changes because jet correlations dominate the correlation structure of p - p collisions.

D. Quadrupole/jet ratio and SS curvatures

Appearance of a SS ridge depends on the condition $16A_{Q,tot}/A_D > 1$, where $A_{Q,tot} = A_Q(\sigma_\phi) + A_Q\{2D\}$. The first term in $A_{Q,tot}$ scales with the AS 1D (jet) peak amplitude A_{1D} , the second is the nonjet quadrupole amplitude. The AS 1D peak model in Fig. 3 (left panel) is a Gaussian with $\sigma_\phi \approx 1$. The *jet-related* quadrupole component of the AS peak is then $2A_Q(\sigma_\phi = 1) \approx 0.1A_D$ [10]. For the curvature discussion in Sec. VII E the 1D Gaussian is approximated as the sum of AS dipole and quadrupole terms only. Requiring an equivalent net curvature at $\phi_\Delta = 0$ leads to $2A_Q(\sigma_\phi) \approx 0.05A_D$. The jet-related quadrupole then includes estimated curvature contributions from higher Fourier components of the AS peak (mainly the sextupole). Nonjet and jet-related quadrupoles (in that order) are shown in both $2A_{Q,tot}$ and $2R_{Q,tot}$ columns of Table I.

The split between $A_Q\{2D\}$ and $A_Q(\sigma_\phi)$ is the dominant uncertainty in characterization of 2D angular correlations in peripheral and central A-A collisions and low-multiplicity p - p collisions, where the nonjet quadrupole amplitude is small relative to the jet amplitudes. The uncertainty in the latter dominates the uncertainty in $16A_Q/A_D$. Combining relative uncertainties in $A_Q\{2D\}$ (25%), $A_Q(\sigma_\phi)$ (10%) and A_D (10%) leads to $16A_Q/A_D \pm 28\%$, included in the corresponding column of Table I.

E. Covariances among model elements

The correlation model of Eq. (4) applied to 2D histograms in this analysis includes four elements: an azimuth dipole A_D , an azimuth quadrupole A_Q , a SS 2D peak A_{2D} and a 1D Gaussian on η_Δ A_2 . The only significant covariance for p - p collisions is between the SS 2D peak and the 1D Gaussian on η_Δ . The two sinusoids are orthogonal to one another and essentially independent of η_Δ whereas the other two elements have large curvatures on η_Δ . The single nontrivial covariance between the two elements strongly varying on η_Δ is not critical to the present analysis of structure on azimuth at larger η_Δ .

F. Possible v_3 contribution

It has recently been suggested that “triangular flow” [26] represented by v_3 (an azimuth *sextupole* correlation component) may contribute to the η -elongated SS 2D peak (“soft ridge”) observed in more-central Au-Au collisions at the RHIC [5, 9]. In such analysis the v_3 amplitude is typically consistent with an $m = 3$ Fourier component of the SS 2D peak, which is about 8% of the SS peak amplitude *averaged over the η_Δ acceptance*. In the case of p - p collisions the v_3 amplitude of a peak narrow on η_Δ would be negligible compared to other structure.

VII. DISCUSSION

This analysis reveals that minimum-bias jet structure at 7 TeV is remarkably similar to that at RHIC energies. The same-side 2D peak amplitude continues to follow the $\log(\sqrt{s})$ energy scaling established between 17 and 200 GeV, while any change in the AS 1D amplitude is much less, consistent with the AS trend at lower energies. Changes in jet structure with applied n_{ch} and p_t cuts at 7 TeV are also similar to those observed in 200 GeV p - p collisions.

Novel structure in the form of a same-side ridge does appear at 7 TeV with application of certain multiplicity and p_t cuts. Does the ridge structure imply novel physics in LHC p - p collisions, or is it simply related to phenomena observed at lower energies? In this section we review jet and quadrupole correlation systematics in p - p and Au-Au collisions and consider how a combination of increased collision energy plus n_{ch} and p_t cuts can lead to a visible SS ridge.

A. Inferred model parameters

Table I presents results from extrapolation of RHIC p - p data to 7 TeV and from modeling CMS data histograms for several cut conditions. The first row summarizes results for p - p collisions at 200 GeV (jet param-

eters) or extrapolated from Au-Au centrality trends (non-jet quadrupole parameter). In general, STAR (A_X) and CMS (R_X) parameters are related by $R_X = 2\pi\Delta\eta A_X \approx 30A_X$, since $\Delta\eta = 4.8$.

In the second row the SS peak and quadrupole amplitudes determined at 200 GeV have been scaled up with energy by factor $R(\sqrt{s}) = 2.3$ [Eq. (10)] inferred from jet and quadrupole energy systematics below 200 GeV. AS dipole amplitude A_D remains the same, consistent with jet structure trends below 200 GeV. The comparison in Fig. 3 indicates that energy extrapolation of 200 GeV jet correlations provides good agreement with 7 TeV data.

In the third row, parameters have been modified in response to the n_{ch} cut. Jet peak amplitudes are further increased by factors 3 (SS) and 4 (AS) and the quadrupole amplitude by factor 6 to match the structure observed in Figs. 4 and 5. In the fourth row, parameters have been further modified in response to the p_t cut. The quadrupole amplitude is unchanged. SS 2D peak amplitude A_{2D} is reduced by factor 1/3 and AS dipole amplitude A_D is reduced by factor 1/2 to match the structure in Fig. 6

Figure 3 tests extrapolation of jet structure from 200 GeV to 7 TeV. The extrapolation is reasonably accurate. Fig. 4 tests the effect of the n_{ch} cut on 7 TeV jet structure compared to the response at 200 GeV. Response to cuts at the two energies is quantitatively similar. Figures 5 and 6 probe the effect of applied cuts on the extrapolated nonjet quadrupole and its possible contribution to formation of the SS ridge.

B. p - p and Au-Au centrality trends

From CMS data we conclude that both $A_Q\{2D\}$ (non-jet quadrupole) and A_D (jets) increase with increasing p - p multiplicity (by factors 6 and 3 respectively for a factor-7 increase in n_{ch}), and that the ratio $A_Q\{2D\}/A_D$ may therefore double). Are such trends consistent with p - p and Au-Au collisions at 200 GeV? We have two sources of information about p - p multiplicity trends at RHIC energies: a) measured 200 GeV p - p systematics and b) arguments by analogy with Au-Au collision centrality.

a. p - p minijet multiplicity systematics at 200 GeV
As noted in Sec. III G selection of high-multiplicity p - p events is expected to bias toward more-central collisions [20]. Two-component analysis of 200 GeV p - p p_t spectra revealed that with a ten-fold increase in multiplicity the jet frequency increased by a factor 50 (almost 100% of collisions include a dijet), which should correspond to a factor-5 increase in per-particle jet correlations (Sec. IV D) [7]. Jet correlation measurements at 200 GeV confirmed that the per-particle jet correlation amplitude increases by about a factor 5 [15, 16].

At 7 TeV the minimum-bias jet frequency is expected to increase relative to 200 GeV by factor $R(7 \text{ TeV}) = 2.3$ to almost 5%. The maximum frequency increase should

then be $50/2.3 = 22$. With a 7-fold increase in event multiplicity we expect the jet correlation amplitude to increase by factor $7(22/7^2) \approx 3$. In Sec. VB we confirm from CMS data that application of a factor-7 high-multiplicity cut does increase the jet correlation amplitude by factor 3.

b. Au-Au quadrupole centrality systematics The nonjet quadrupole in A-A collisions below 200 GeV depends only on collision energy and initial geometry in the form b/b_0 (the relative geometry of intersecting spheres), not on absolute system size. The two trends are factorized as in Eq. (9) [12]. We argue by analogy between p - p and Au-Au centrality that the same increase in p - p centrality which leads to increased jet production should produce a corresponding quadrupole increase.

The measured nonjet quadrupole amplitude is expressed in terms of A-A centrality parameters by $A_Q\{2D\} = \rho_0(b)v_2^2\{2D\} \propto n_{bin}\epsilon_{opt}^2$ [12]. The AS 1D peak amplitude) scales with A-A centrality as $A_D/2 \propto \rho_0(b)j^2 \propto \nu/(1+x(\nu-1)) \approx \nu$ [9]. The Glauber parameters are related by $n_{bin} \sim \nu^4$ and $n_{part} \sim \nu^3$. Thus, A_Q/A_D scales with Au-Au centrality as $\nu^3 \sim n_{part}$, which increases by a factor 50 up to the maximum of A_Q beyond which the rapid decrease of $\epsilon_{opt}^2(b)$ dominates.

We assume that ϵ_{opt}^2 changes (increases) slowly with n_{ch} in p - p collisions and that the quadrupole amplitude increases *at least as fast* as the AS 1D peak amplitude and probably faster with n_{ch} based on Au-Au centrality systematics. A nonjet quadrupole increase twice the jet increase as required by CMS data (SS curvature) is thus consistent with measured p - p and Au-Au centrality trends at RHIC energies.

C. p - p minijet response to p_t cuts

In Sec. VC we observed that with $p_t \in [1, 3]$ GeV/c cuts imposed the 7 TeV SS peak amplitude is reduced by factor 1/3 and the AS ridge is reduced by factor 1/2. As noted in Sec. IVD in p - p correlations on $y_t \times y_t$ at 200 GeV [15, 16] SS jet correlations extend down to $p_t = 0.3$ GeV/c, with mode at 1 GeV/c. Nearly half the SS-correlated pairs appear below the mode. In contrast, AS correlations are cut off near 0.7 GeV/c due to initial-state k_t effects. A smaller fraction of AS pairs appears below 1 GeV/c. The p_t cut systematics at 7 TeV are thus consistent with 200 GeV jet structure on $y_t \times y_t$. With the high-multiplicity cut (more-central p - p collisions) the SS peak azimuth width decreases from 0.9 to 0.65. With the high- p_t cut the SS 2D azimuth width is further reduced to 0.55 leading to a symmetric SS jet peak. Similar reductions in SS peak azimuth width are observed at 200 GeV and are consistent with centrality trends in Au-Au collisions [9].

D. Pb-Pb v_2 measurements at 2.76 TeV

v_2 data for 2.76 TeV Pb-Pb collisions have recently been reported [27]. The p_t -differential $v_2(p_t, b)$ data fall within 10% of 200 GeV data (Fig. 2 of Ref. [27]). The comparison is made with $v_2\{4\}$ (four-particle cumulant method) which is less sensitive to jet structure (nonflow).

p_t -integral $v_2(b)$ data at 2.76 TeV for more-central Pb-Pb collisions (Fig. 3 of Ref. [27]) are 30% higher than STAR data at 200 GeV, apparently due to p_t spectrum shape changes (larger mean p_t). However, for more-peripheral collisions the 2.76 TeV data, for v_2 methods less sensitive to jet structure ($v_2\{4\}$, Lee-Yang zeroes or LYZ), appear to converge with the 200 GeV data. Energy dependence of the 20-30% centrality bin (Fig. 4 of Ref. [27]) reflects the 30% increment in $v_2(b)$, but data for more-peripheral collisions exhibits a substantially smaller increase.

For more-peripheral A-A and p - p collisions nonjet quadrupole measure $A_Q\{2D\} = \rho_0 v_2^2\{2D\} \propto R(\sqrt{s_{NN}})$ above 13.5 GeV. Between 62 and 200 GeV $\rho_0(b)$ increases by only 10% as $R(\sqrt{s_{NN}})$ increases by factor 1.75 and v_2^2 increases substantially. At higher energies we observe that $\rho_0(b) \rightarrow \propto R(\sqrt{s_{NN}})$ as particle production becomes jet dominated, and $v_2^2 \rightarrow$ constant for more-peripheral A-A collisions. In more-central A-A collisions changes in the p_t spectrum (greater minijet production, harder spectrum) may cause p_t -integral $v_2^2(b)$ to exceed that trend significantly, whereas differential $v_2^2(p_t, b)$ does not change significantly with collision energy. Extrapolation of the nonjet quadrupole amplitude $A_Q\{2D\}$ in p - p collisions above 200 GeV according to Eq. (10) is thus consistent with Pb-Pb measurements at the LHC.

E. Azimuth curvatures and SS ridge phenomenon

This analysis tests the hypothesis that the ridge observed in p - p data at 7 TeV results from a competition between two curvature contributions on ϕ_Δ within $|\eta_\Delta| > 2$ (excluding the SS 2D peak). A visible ridge may appear when the sum of correlation structure near $\phi_\Delta = 0$ becomes significantly concave downward (negative curvature). In minimum-bias p - p collisions at 7 TeV and all p - p collisions at RHIC energies we observe only a positive curvature in that region (no visible ridge).

The dominant structures within $|\eta_\Delta| > 2$ are the AS dipole $\cos(\phi_\Delta - \pi)$ and the azimuth quadrupole $\cos(2\phi_\Delta)$. The curvature of $\cos(2\phi_\Delta)$ at $\phi_\Delta = 0$ is four times the curvature of $\cos(\phi_\Delta - \pi)$ with opposite sign. Like the CMS ridge, the 200 GeV nonjet quadrupole and AS 1D jet peak are insensitive to charge combination, with equal amplitude for like-sign and unlike-sign charge pairs [6]. The SS net curvature is then determined by the coefficients of two sinusoids— $A_D/2$ for the dipole and $2A_Q$ for the quadrupole. Zero net curvature corresponds to $4 \times 2A_Q = A_D/2$ or $16A_Q/A_D = 1$. That ratio is included in Table I. A ridge (negative curvature) is ob-

served if the ratio is significantly greater than one. A small relative change in correlation amplitudes may result in qualitative appearance or disappearance of a SS ridge.

As revealed in Table I the consequence of increased collision energy (factor 2) plus applied p_t (factor 2) and n_{ch} (factor 1.5) cuts at 7 TeV increases the nonjet quadrupole amplitude relative to the AS dipole by an overall factor 6, changing the SS curvature sign and producing a visible SS ridge. In effect, the SS azimuth curvature functions as a comparator, switching states from valley to ridge as one correlation amplitude changes relative to another.

F. Relevance of the Au-Au SS ridge to p - p collisions

The jet-related SS “ridge” observed in more-central Au-Au collisions at RHIC energies could be compared with the SS ridge observed in 7 TeV p - p collisions. Two manifestations of the Au-Au ridge phenomenon are notable: (i) η elongation of a monolithic SS peak accurately described by a single 2D Gaussian [5, 9] and (ii) development of a seemingly separate ridge-like structure beneath a symmetric 2D jet peak with certain applied p_t cuts [2]. Item (i), well established for “untriggered” (no p_t cuts) jet correlations and for some combinations of p_t cuts, has been referred to as a “soft ridge,” although there is no separate ridge per se. Item (ii) is inferred from other combinations of p_t cuts (“trigger-associated” dihadron analysis).

Elongation of the p_t -integral SS 2D peak (i) undergoes a sharp transition on centrality in A-A collisions (both Au-Au and Cu-Cu collisions) [9]. For more-peripheral A-A and p - p collisions the SS peak is strongly elongated in the ϕ direction (3:2) [16]. For more-central collisions the SS peak transitions to strong elongation in the η direction (3:1) [5, 9]. The (sharp) transition in peak properties occurs within a small centrality interval. Variation of SS jet peak structure with p_t cuts (ii) is complex, depending strongly on different charge-sign combinations, hadron p_t and hadron species. Assignment of certain aspects of peak structure to a distinct ridge phenomenon for some p_t cuts is questionable.

We observe that for p - p collisions the minimum-bias SS 2D peak η and ϕ widths have the same value at 7 TeV as at 200 GeV and are reduced slightly with applied cuts just as at lower energies. Thus, item (i) η broadening is not observed. The appearance of a SS “ridge” in CMS p - p data for some cut combinations could be associated with item (ii). However, the absence of item (i) and consistency with known azimuth quadrupole systematics makes interpretation (ii) unlikely. There is thus no indication from p - p data that the CMS ridge is directly associated with the SS 2D (jet) peak. A more definitive resolution may come from systematic study of Pb-Pb centrality systematics.

The $R(\sqrt{s})$ trend Eq. (10) inferred from angular correlation energy systematics below 200 GeV [12, 28] also

describes NSD p - p particle densities above 200 GeV. The NSD value $dn_{ch}/d\eta = 2.5$ at 200 GeV combined with $R(7 \text{ TeV}) = 2.3$ predicts 5.75 consistent with the CMS measurement ~ 5.8 [8]. The CMS high-multiplicity cut produces a 7-fold increase over the NSD angular density to $dn_{ch}/d\eta = 40$. In a study of 200 GeV p - p spectra [7] the multiplicity variation included a 10-fold increase (to $dn_{ch}/d\eta = 25$). The maximum particle density studied at 200 GeV is thus 60% of the maximum at 7 TeV. RHIC and LHC p - p particle densities are directly comparable, and much smaller than densities achieved in more-central Au-Au collisions at RHIC.

VIII. SUMMARY

Direct A-B comparisons between CMS 2D angular correlations from 7 TeV p - p collisions and parametrizations of 200 GeV p - p correlations with identical histogram formats provide a quantitative model description of the CMS data. Model fits reveal that 200 GeV and 7 TeV minimum-bias p - p collisions are remarkably similar. Midrapidity intrajet (same-side jet peak) correlation amplitudes and multiplicity densities increase by factor $R(\sqrt{s} = 7 \text{ TeV}) = 2.3$ over those measured at 200 GeV. Minimum-bias correlation structure is otherwise similar. Response to n_{ch} and p_t cuts is also consistent with trends at 200 GeV. Changes in jet-like correlation amplitudes and same-side 2D peak widths are quantitatively consistent with STAR p - p correlation analysis at 200 GeV.

The single novel manifestation at 7 TeV is the appearance of a same-side “ridge” for certain multiplicity and p_t cuts. It is conjectured that the ridge structure in 7 TeV p - p collisions may be similar to that observed in more-central Au-Au collisions at 200 GeV, interpreted by some to indicate formation of a dense QCD medium.

However, extrapolation of nonjet quadrupole systematics measured in RHIC Au-Au collisions to 7 TeV p - p collisions predicts a significant quadrupole amplitude in minimum-bias p - p collisions. Although the consequences to the quadrupole of multiplicity and p_t cuts applied in the CMS analysis cannot be predicted quantitatively, a six-fold increase over the minimum-bias quadrupole prediction fully accounts for the same-side ridge structure in 7 GeV p - p collisions. A modest increase in the quadrupole amplitude (enhanced by energy increase and multiplicity cuts) relative to the away-side ridge (reduced by p_t cuts) can reverse the curvature sign near the azimuth origin, resulting in a visible ridge structure.

We conclude that the same-side ridge observed at 7 TeV is consistent with p - p and Au-Au measurements at 200 GeV and below, including responses to applied cuts. The azimuth quadrupole clearly apparent in more-central Au-Au collisions at RHIC is directly visualized in p - p angular correlations at the LHC as a curvature reversal resulting from consequences of larger collision energy combined with kinematic cuts. LHC data offer the possibility to study the systematics of the azimuth quadrupole in el-

elementary collisions. Model fits can be applied as in cited references to increase sensitivity to nonjet quadrupole structure. By such means the azimuth quadrupole may be better understood as a QCD phenomenon.

We greatly appreciate extensive discussions on two-

particle correlations in nuclear collisions over a number of years with Lanny Ray, Jeff Porter and Duncan Prindle. This work was supported in part by the Office of Science of the U.S. DOE under grant DE-FG03-97ER41020.

-
- [1] CMS Collaboration, JHEP **1009**, 091 (2010), arXiv:1009.4122.
- [2] B. I. Abelev *et al.* (STAR Collaboration), Phys. Rev. C **80**, 064912 (2009).
- [3] T. Hirano and M. Gyulassy, Nucl. Phys. A **769**, 71 (2006).
- [4] L. P. Csernai, J. I. Kapusta and L. D. McLerran, Phys. Rev. Lett. **97**, 152303 (2006).
- [5] J. Adams *et al.* (STAR Collaboration), Phys. Rev. C **73**, 064907 (2006).
- [6] J. Adams *et al.* (STAR Collaboration), Phys. Lett. B **634**, 347 (2006).
- [7] J. Adams *et al.* (STAR Collaboration), Phys. Rev. D **74**, 032006 (2006).
- [8] V. Khachatryan *et al.* (CMS Collaboration), Phys. Rev. Lett. **105**, 022002 (2010).
- [9] M. Daugherty (STAR Collaboration), J. Phys. G **35**, 104090 (2008).
- [10] T. A. Trainor, Phys. Rev. C **81**, 014905 (2010).
- [11] T. A. Trainor, R. J. Porter and D. J. Prindle, J. Phys. G **31**, 809 (2005).
- [12] D. T. Kettler (STAR collaboration), Eur. Phys. J. C **62**, 175 (2009).
- [13] D. Kettler (STAR Collaboration), J. Phys. Conf. Ser. **270**, 012058 (2011).
- [14] D. Kettler (STAR Collaboration), PoS **CERP2010**, 011 (2010).
- [15] R. J. Porter and T. A. Trainor (STAR Collaboration), J. Phys. Conf. Ser. **27**, 98 (2005).
- [16] R. J. Porter and T. A. Trainor (STAR Collaboration), PoS **CFRNC2006**, 004 (2006).
- [17] T. A. Trainor, Int. J. Mod. Phys. E **17**, 1499 (2008).
- [18] T. A. Trainor and D. T. Kettler, Phys. Rev. C **83**, 034903 (2011).
- [19] T. A. Trainor and D. J. Prindle, hep-ph/0411217.
- [20] L. Frankfurt, M. Strikman and C. Weiss, Phys. Rev. D **69**, 114010 (2004).
- [21] T. A. Trainor, Phys. Rev. C **80**, 044901 (2009).
- [22] X.-N. Wang, Phys. Rev. D **46**, R1900 (1992); X.-N. Wang and M. Gyulassy, Phys. Rev. D **44**, 3501 (1991).
- [23] T. A. Trainor, J. Phys. G **37**, 085004 (2010).
- [24] P. Huovinen and P. V. Ruuskanen, Ann. Rev. Nucl. Part. Sci. **56**, 163 (2006).
- [25] T. A. Trainor, Mod. Phys. Lett. A **23**, 569 (2008).
- [26] B. Alver and G. Roland, Phys. Rev. C **81**, 054905 (2010).
- [27] K. Aamodt *et al.* (The ALICE Collaboration), arXiv:1011.3914.
- [28] J. Adams *et al.* (STAR Collaboration), J. Phys. G **33**, 451 (2007).